On the Interaction of Phosphines with High Surface Area Mesoporous Silica

Hélène Staub,[a,b,c] *Iker Del Rosal,*[d] *Laurent Maron,**[d] *Freddy Kleitz**[a,b] *and Frédéric-Georges Fontaine**[a,c]

[a] Department of Chemistry, 1045 Avenue de la Médecine, Université Laval, Québec (Qc), G1V 0A6 (Canada), Fax: +1-418-656-7916

E-mails: frederic.fontaine@chm.ulaval.ca; freddy.kleitz@chm.ulaval.ca;

[b] Centre de recherche sur les matériaux avancés (CERMA), Université Laval

[c] Centre de recherche sur la propriété des interfaces et de la catalyse (CERPIC), Université Laval

[d] Université de Toulouse, INSA, UPS, CNRS-UMR5215, LPCNO, 135 Avenue de Rangueil, 31077 Toulouse, France.

E-mail: laurent.maron@irsamc.ups-tlse.fr

This is the peer reviewed version of the following article: [On the Interaction of Phosphines with High Surface Area Mesoporous Silica, J. Phys. Chem. C 2012, 116, 25919−25927], which has been published in final form at [10.1021/jp309900n].

Abstract

To increase the efficiency and selectivity of homogeneous catalysts, particularly useful in the synthesis of fine chemicals and drugs, fine tuning of the steric and electronic properties of the complexes can be achieved by modification of the ligands in the coordination sphere of the metal center. Considerable efforts have been devoted in order to immobilize such well-defined catalysts on solid substrates, e.g., silica, to facilitate catalysts' recovery and to reduce contamination of desired products by metallic impurities. However, the presence of the silica surface can play a very important role in tuning the electronic properties of the metal, its steric environment, or in participating in the reactivity of the complex. In this context, several moieties have been used to anchor metallic catalysts on surfaces, but one of the most interesting is phosphine. Herein, we report on the addition of PPh_2Cl which leads to the grafting and the oxidation of the phosphine species, even in absence of oxygen, and that the nature of the surface plays an important role in secondary interactions, e.g., hydrogen bonding, and modifies the spectroscopic properties of the functional groups on the surface. In particular, the chemical shift of the phosphorous resonance in the ^{31}P NMR spectra is altered by hydrogen bonding between available silanol or water molecules present on the silica surface and the phosphorous oxide. The DFT models developed for this process are in direct accordance with the experimental results and demonstrate firmly that the oxidation of the phosphine after grafting of $ClPR_2$ is highly favored thermodynamically and occurs with the formation of Si-Cl bonds on the surface. Passivation of the surface with hexamethyldisilazane limits the extent of the H-bonding between the surface and the oxide, but also leads to some substitution reaction between bound phosphorous species and the trimethylsilyl (TMS) moieties. These findings

offer new knowledge critical to fully ascertain the environment and the stability of immobilized phosphine-containing catalytic systems and, thus, further broaden the range of their reactivity.

Introduction

Global interest in green chemistry has led to great initiatives in order to reduce undesirable by-products generated in industrial-scale chemical reactions, notably using catalysis. In order to increase the efficiency and selectivity of homogeneous catalysts, particularly useful in the synthesis of fine chemicals and drugs, fine tuning of the steric and electronic properties of the complexes can be done by modification of the ligands in the coordination sphere of the metal. However, one of the major limitations of homogeneous catalytic systems is often the need for purification steps in order to remove residual metals.[1] To solve this problem, considerable effort has been done in order to immobilize well-defined catalysts on solid substrates to facilitate the catalysts' recovery and to reduce the contamination of desired products by metallic impurities.[2] Although many solid supports have been used and developed, one of the most desirable is silica.[3] Silica materials are cheap, robust, and inert under most synthetic and catalytic conditions, but most importantly, the presence of silanol moieties on the surface allows for easy functionalization of the surface by condensation reactions or protonolysis. In addition, there are nowadays many known synthetic procedures to generate a large array of well-defined structures and morphologies for silica that can provide a wide range of physical properties of interest for fine-tuning catalytic systems.[4]

Several moieties have been used to anchor metallic catalysts on surfaces, but one of the most interesting is phosphine.[5] Although other methodologies have been developed, the incorporation of phosphines on silica has been mostly designed through the post-functionalization of surfaces by tailored molecules containing a terminal trialkoxy- or trichlorosilane.[6] One of the advantages of the linker is to

increase the flexibility of the bound complex and to limit the interactions with the surface. However, in the context of catalysis, the presence of the silica surface can play a very important role in tuning the electronic properties of the metal, its steric environment, or in participating in the reactivity of the complex. For example, Schrock and Copéret used silica as a support for molybdenum carbenes and have demonstrated that the support acts as a ligand, replacing one of the alkoxide groups in the analogous homogeneous Schrock catalyst.[7] In this regard, it could be tempting to incorporate a phosphine moiety directly on the surface of silica without the presence of a linker, so to act as a very bulky phosphine. To our knowledge, the only mention of a phosphine being directly immobilized on a silica surface through a Si-O-PR_2 linkage has been reported by Verdonck *et al.* where they used $ClPPh_2$ to generate a diphenylphosphine moiety on silica that was further used as ligand to coordinate $RuCl_3$.[8] According to FTIR and XPS studies, it was proposed that the addition of the chlorodiphenylphosphine yielded discrete Si-O-PPh_2 moieties on the surface that could be later used as ligands for coordination of the ruthenium center in a monodentate or bidentate fashion. However, this report contrasts drastically with the work carried out by Morrow and Lang[9] on the chemisorption of Me_2PCl where they showed IR evidence of generation of Si-O-$P(O)Me_2$ on the surface, resulting from the oxidation of the phosphine by the surface according to a general equation (eq. 1) summing up to:

2 [Si]OH + 2 PMe_2Cl → [Si]Cl + Me_2PH + HCl + [Si]$OP(O)Me_2$ (eq. 1)

These contrasting results led us to investigate more thoroughly this reaction using multi-nucleus nuclear magnetic resonance (NMR) spectroscopy, attenuated total reflection infrared spectroscopy (ATR-IR) and density functional theory methods (DFT) in order to understand the actual behaviour of $ClPPh_2$ immobilized on silica, notably to see whether the presence of an aryl group rather than an alkyl group could help preventing the oxidation of the phosphorous moiety by the surface. We wish to report that the

addition of PPh_2Cl to mesoporous silica supports leads to the grafting and the oxidation of the phosphine, even in absence of oxygen, and that the nature of the surface plays an important role in secondary interactions, such as hydrogen bonding, modifying the spectroscopic properties of the functional groups on the surface.

Results and discussion

Grafting of Ph_2PCl on SBA-15 and MCM-41 mesoporous silica

For this study, ordered mesoporous SBA-15 and MCM-41 silica materials were selected as hosts for the grafting of $ClPPh_2$. SBA-15 and MCM-41 were synthesized according to optimized procedures developed by Choi *et al.* in 2003[10] and by Grün *et al.* in 1999,[11] respectively. The typical nitrogen adsorption-desorption isotherms of these two mesoporous materials are presented in Figure S1 (Supporting Information) with their textural parameters, all being in agreement with previous reports.[12] In a first series of experiments, the addition of $ClPPh_2$ to the mesoporous SBA-15 and MCM-41 materials was carried out under reflux conditions for 4 hours under a dry nitrogen atmosphere yielding materials designated as **SBA-Ph** and **MCM-Ph**, respectively. Both materials were analyzed using $^{13}C\{^1H\}$ CP/MAS NMR spectroscopy and exhibited very similar spectroscopic features with a single resonance at 129 ppm typical for the phenyl groups on the phosphorous (Figure 1). $^{31}P\{^1H\}$ MAS NMR spectroscopy also revealed simple spectroscopic features with a single resonance at 22 ppm for both materials (Figure 2). It therefore seems that the nature of the solid substrate does not affect the bonding mode of the phosphorous moiety, although the signal of **SBA-Ph** is significantly larger than that observed for **MCM-Ph** ($w_{1/2}$ = 1300 Hz and 1000 Hz, respectively). The two materials were then either

exposed to air for a period of 12 hours or Soxhlet-extracted under refluxing conditions in CH_2Cl_2 under air for a period of 20 hours, yielding the materials **SBA/MCM-Ph-O$_2$** and **SBA/MCM-Ph-sox**, respectively. Although all of the species exhibit very similar spectroscopic features to the parent materials according to $^{13}C\{^1H\}$ CP/MAS NMR spectroscopy (Figures S2, Supporting Information), the $^{31}P\{^1H\}$ MAS NMR signature of the four materials differ significantly (Figure 3). In the case of **SBA-Ph-O$_2$** and **SBA-Ph-sox** materials, a single sharp resonance at 29 ppm was observed, downfield from the materials **SBA/MCM-Ph** at 22 ppm. On the other hand, both materials **MCM-Ph-O$_2$** and **MCM-Ph-sox** also exhibit the same species at 29 ppm, but have in addition another resonance at 25 ppm in somewhat lower intensity that the former resonance.

(Insert Figures 1-3)

Because of the lack of model compounds available to compare these chemical shifts with, DFT was used to probe the possible interactions between the phosphorous moiety and the support materials and to provide predictive values for the ^{31}P chemical shift of these species. In a previous work,[13] based on the rigidity of the ligand, the surface density of silanol groups and the silanol IR frequencies of hydroxyl groups, five realistic molecular models of silica surface (mainly amorphous silica thermally treated at 200°C) were defined to describe satisfactorily the presence of different silanol groups onto a SiO_2 surface (isolated, vicinal, germinal or a mixture of vicinal and germinal silanol groups). In order to model the mesoporous materials, these five different surface models were used to account for different silanol coverage of the surface (see Figure 4 and Figures S3 and S4, Supporting information). In all of the cases, two silicon atoms represent the emerged part of the silica surface and thus the different silanol groups. The emerged part is surrounded by a layer built around four silicon atoms, themselves connected to O–SiH_3 groups which are chosen as model to mimic the continuity of the surface. Finally, a second

layer formed by two silicon atoms, connected by a siloxane bridge, is added to increase the rigidity of the model. Both silicons are connected to hydroxyl groups in order to saturate the model. In a same way, SiH_3 groups are added, on the emerged part of the silica, to saturate the lateral siloxane bridges formed during the dehydroxylation reaction of the silica surface.

(Insert Figure 4)

Table 1. Relative Gibbs-free energies (kcal.mol^{-1}) and $^{\{31\}}$P NMR (ppm) of the intermediates in the grafting reaction and oxidation of Ph_2PCl on the **ac**, **c** and **b** $SiO_{2\text{-}200}$ models. The labels **A** to **B** refer to the intermediates shown in Figure S5.

	Grafting reaction		Oxidation reaction					
	ΔrG	$^{\{31\}}$P	ΔrG	$^{\{31\}}$P	ΔrG	$^{\{31\}}$P	ΔrG	$^{\{31\}}$P
c model	(**A**)$_c$		(**B**)$_c$		-		-	
	5.1	120	-80.0	32				
ac model	(**A**)$_{ac}$		(**B**)$_{ac}$		(**B**)'$_{ac}$		-	
	3.9	122	-84.2	38	-79.5	34		
b model	(**A**)$_b$		(**B**)$_b$		(**B**)'$_b$		(**B**)'$_b$	
	5.6	141	-85.9	32	-79.1	36	-80.0	41

However, since all of the models displayed similar trends, only the results of the $Si_{12}O_{20}H_{16}$ model (**ac** model) are reported here. In a first pathway, the grafting of Ph_2PCl to one silanol moiety was explored. The resulting product (**A**) was shown to be slightly endergonic with a ΔrG of +3.9 kcal.mol^{-1}.

On the other hand, the oxidation reaction, to generate the phosphine oxide (**B**), is highly favored by 84.2 kcal.mol^{-1}. It was also experimentally demonstrated that the addition of a trialkyl- or triarylphosphine on mesoporous silica could lead to the formation of a phosphonium species either by the presence of residual HCl or by a silanol having a significant Broensted acidity.[14] The phosphonium species resulting from the protonation of **A** was also evaluated as a potential species grafted on silica (**C**) (see Figures S6 and S7, Supporting Information). Interestingly, the calculated ^{31}P NMR chemical shift values for species for **A, B**, and **C** are quite distinct, at 122, 38, and 53 ppm, respectively, allowing a possible discrimination of the species using NMR spectroscopy.

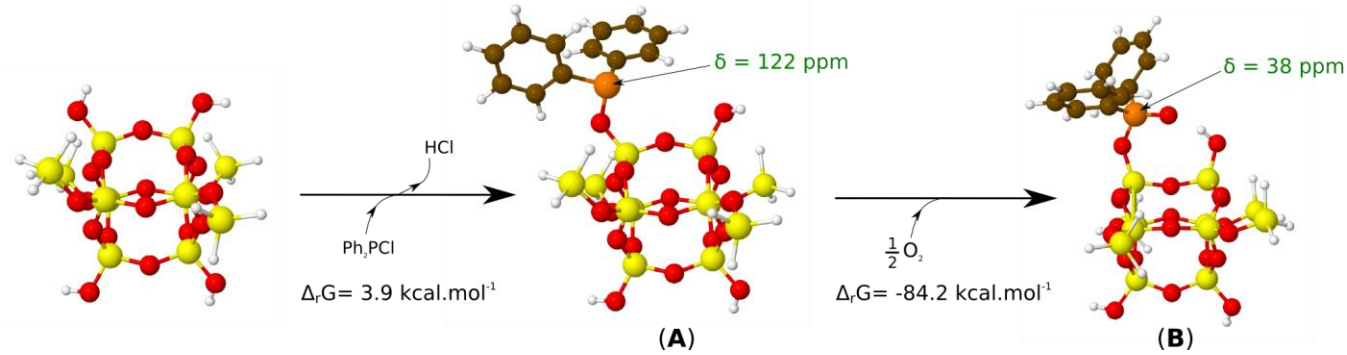

Scheme 1. Reaction of the supported phosphine species with HCl.

Therefore, according to the DFT models, it is more likely that in all **SBA/MCM-Ph** materials synthesized, even in the absence of air, phosphine oxide species are generated, which would support Morrow's report.[9] The oxidation process as proposed by Morrow was modeled using computational chemistry and is described in Scheme 1. Once the grating of the surface to generate **A**, it is possible for the bound species to react with the outcoming HCl to generate $Ph_2P(H)(O)$ and generate a $(RO)_3SiCl$ moiety (ΔrG = -1.5 kcal.mol^{-1}) (See Scheme 2). The diphenylphosphine oxide can subsequently react with diphenylphosphine chloride to generate PPh_2PH and the oxide of diphenylphosphine chloride (ΔrG

= -6.7 kcal.mol^{-1}), which in turn will react with the silanol groups to generate the silica-bound phosphine oxide (ΔrG = -3.8 kcal.mol^{-1}) (Scheme 3).

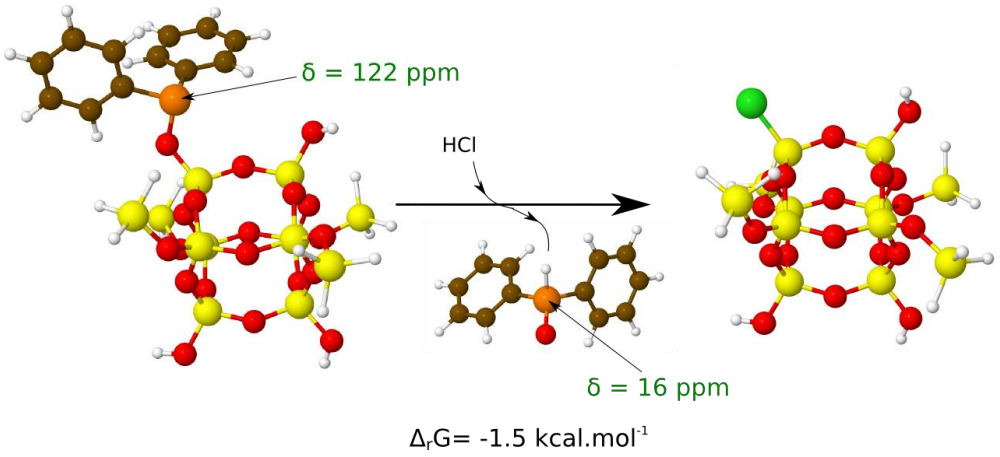

Scheme 2. Generation of a chlorinated silica support from a grafted phosphine.

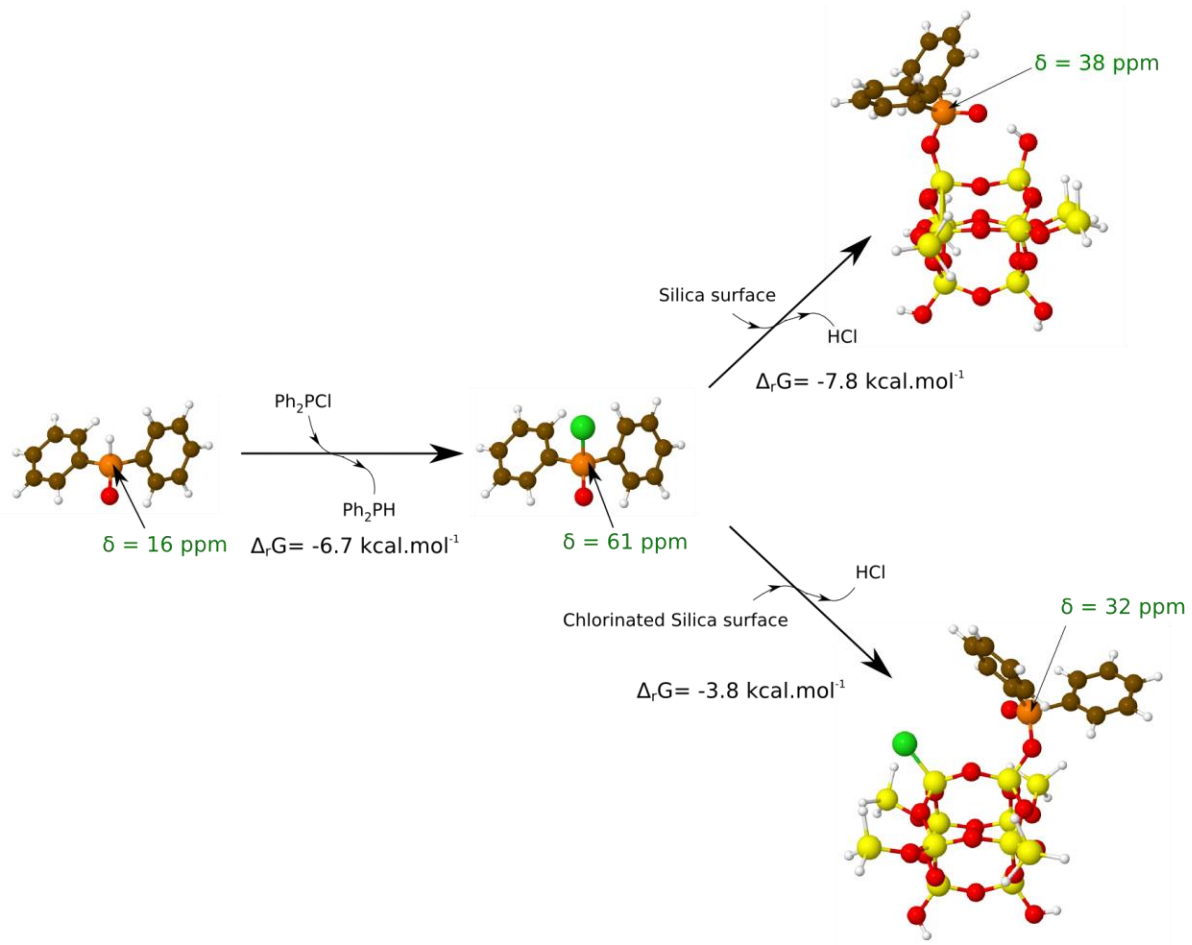

Scheme 3. Generation of a supported phosphine oxide from $Ph_2P(O)Cl$.

Table 2. Relative Gibbs-free energies (kcal.mol^{-1}) and $^{\{31\}}P$ MAS NMR (ppm) of the intermediates in the generation of silica-bound phosphine oxide on the **ac**, **c** and **b** $SiO_{2\text{-}200}$ models via the formation of an $Ph_2P(H)(O)$ complex.

	Chlorination of the silica surface	Formation of $Ph_2P(O)(Cl)$	Grafting of $Ph_2P(O)(Cl)$ on dehydroxylated silica surface.		Grafting of $Ph_2P(O)(Cl)$ on chlorinated silica surface.	
	ΔrG	ΔrG	ΔrG	$^{\{31\}}P$	ΔrG	$^{\{31\}}P$

c model	-2.5	-6.7	-2.4	32	-	-
ac model	-1.5	-6.7	-7.8	38	-3.8	32
b model	-2.4	-6.7	-7.7	32	-2.8	36

Although these results are strong arguments in favor of the oxidation of the phosphine on the surface, it does not explain the nature of the two similar, but spectroscopically different, species observed by ^{31}P NMR upon exposure to air. A more in depth look at the DFT data does show that two possible conformations are possible for the grafted phosphine oxide on the surface, one involving a hydrogen bond with a surface silanol and another without such interaction. Looking at the calculated ^{31}P NMR shift, it can be observed that the hydrogen bound species (δ = 38) is at lower field than the free species (δ = 32) by 6 ppm (see Scheme 3), a difference that is close to the spectroscopic data observed for the materials reported above. Therefore, prior to exposition to air, the addition of chlorodiphenylphosphine to silica would lead to a high coverage of phosphines on silica and of Si-Cl on the surface, but at the same time would lead to an important removal of the silanol and water coverage on the surface, which could get rehydrated upon exposure to air, possibly by hydrolysis of the Si-Cl moiety.

In order to probe this possibility, ATR-IR of the materials synthesized prior and after exposure to air was obtained (Figure 5). It can be seen that the characteristic bands for the silanols and water coverage are more or less absent from the materials after functionalization under inert atmosphere, but that after exposure to air, one large band centered at 3400 cm^{-1} and an additional one at 3650 cm^{-1} are present, confirming that the silanol and/or water coverage is drastically increased, which could explain the spectroscopic difference between both phosphine-containing species, which are observed using NMR spectroscopy.

(Insert Figure 5)

Passivation of the silica surface

In order to support the idea that the source of the phosphorous chemical shift originated from the hydrogen bond with silica materials, passivation of the surface using hexamethyldisilazane (HMDS) was carried out on materials **SBA-Ph** and **MCM-Ph** to yield materials **SBA*-Ph** and **MCM*-Ph**, respectively**.**[14a] Both the ^{13}C CP/MAS and ^{29}Si MAS NMR spectroscopic data confirm that the addition of the TMS groups has been successful, with the characteristic resonances at -2 ppm and 12 ppm in the ^{13}C and ^{29}Si NMR spectra, respectively (Figures S8 and S9, Supporting Information). For all materials, a single and large resonance is observed by ^{31}P NMR spectroscopy at 21 ppm, suggesting that the phosphorous environment has not been significantly modified after passivation of the surface (Figure 6). Upon exposure to air, the chemical shift for the phosphorous of the **SBA*-Ph** material is downfield by 3 ppm, at 24 ppm, whereas no difference in the chemical shift is observed for the **MCM*-Ph** material (Figure 7). These results contrast somewhat with the observed results for the non passivated samples, but are not surprising when keeping in mind that silanol density could be different in SBA-15 materials compared to MCM-41 since the surface area of the former sample is significantly higher and that the presence of inter-wall microporosity in SBA-15 can affect the distribution of reagents on the surface.[15] The ATR-IR results shown in Figure 8 demonstrate once more that upon exposure to air, the OH content in both **MCM*-Ph** and **SBA*-Ph** is somewhat enhanced, but that the effect is much less important than the one observed for **MCM-Ph** and **SBA-Ph**, as expected for the more hydrophobic passivated samples.

Carbon, hydrogen and chloride elemental analyses on four selected materials (**SBA-Ph**, **SBA-Ph-O$_2$**, **SBA*-Ph**, **SBA*-Ph-O$_2$**) were carried out.[16] In **SBA-Ph**, the carbon, hydrogen and chlorine

contents were found to be 10.4, 1.0, and 0.7%, respectively. Albeit lower than expected, the chlorine content confirms that some residual Cl remains, therefore supporting the presence of Si-Cl moieties. After the exposure to air, however, no detectable amount of Cl could be observed, suggesting that the later moieties could undergo hydrolysis to restore the Si-OH groups and releasing HCl which is removed after washing. Another interesting feature of **SBA-Ph-O$_2$** is the significantly lower amount of carbon on the surface (9.9%), whereas the hydrogen content remained more or less constant. Such values could be once more attributed to the presence of water on the surface. Surprisingly, whereas a larger carbon content would be expected from addition of trimethylsilyl groups, **SBA*-Ph** materials exhibit a slightly lower carbon content than **SBA-Ph** (9.1 and 10.4%, respectively), but higher hydrogen content (1.6 and 1.0%, respectively). Such result would suggest that the phosphines could partially be displaced by a TMS group upon passivation. Once more, DFT was used to monitor whether such displacement was likely to occur, using TMSCl as a modeled silylation agent (see Figure S10 for details). Accordingly, this transformation is slightly exothermic, by a factor of -0.5 kcal.mol^{-1} as shown in Scheme 4, therefore suggesting that such transformation could indeed take place. Upon exposure to air, the **SBA*-Ph-O$_2$** material exhibits a slightly smaller carbon content (0.2%) and higher hydrogen content (0.1%), which could be attributed to some water incorporation, as supported by the above results, but the effect remains negligible compared to **SBA-Ph**.

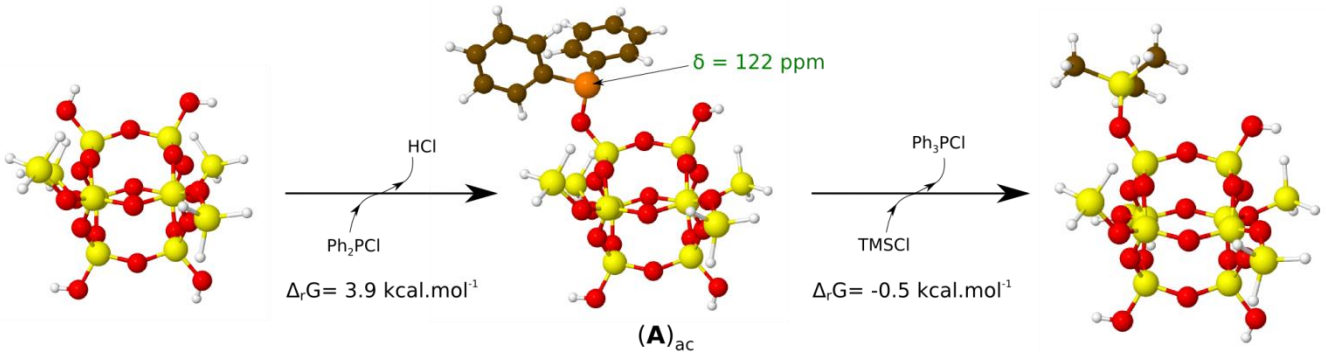

Scheme 4. Exchange of a bound phosphine oxide for a trimethylsilyl group on the silica surface.

Conclusion

The introduction of chlorodialkylphosphines on mesoporous silica leads to the formation of supported -$P(O)R_2$ moieties, as evidenced by solid-state NMR spectroscopy. A factor that modifies the chemical shift of the phosphorous resonance in the ^{31}P NMR spectra is hydrogen bonding between available silanol or water molecules present on the silica surface and the phosphorous oxide. After grafting of the phosphine, a low coverage of EOH (E = H or SiR_3) on the surface was observed and could be correlated to a shielding of the ^{31}P NMR resonance, which shifts to higher field upon exposure to air and moisture. The DFT models developed for this process are in direct accordance with the experimental results and demonstrate firmly that the oxidation of the phosphine after the grafting procedure of $ClPR_2$ is highly favored thermodynamically and occurs with the formation of Si-Cl bonds on the surface. Passivation of the surface with hexamethyldisilazane limits the extent of the hydrogen bonding between the surface and the oxide, but also leads to some substitution reaction between bound phosphorous species and the TMS moieties, as confirmed by the elemental analysis results. In conclusion, we believe that these findings offer new understanding regarding surface interactions between mesoporous silica supports and phosphine species. This knowledge is essential to fully ascertain the environment and the stability of immobilized phosphine-containing catalytic systems and, thus, further broaden the range of their reactivity. In particular, it should be useful to promote the use of metal-phosphorous coordination chemistry on solid surfaces, involving more oxophilic species such as early transition metals and lanthanides, with prospects for catalytic reactions or metal sequestration/extraction applications.[17]

Experimental section

Materials. All grafting manipulations were carried out under an atmosphere of nitrogen, using standard Schlenk and glove box techniques. All support materials were outgassed under vacuum overnight, at 200 °C. Dry dichloromethane and toluene were distilled from sodium/benzophenone.

SBA-15 silica support. Mesostructured SBA-15 silica material was prepared under aqueous acidic conditions using poly(alkylene oxyde)-based triblock copolymer Pluronic P123 ($EO_{20}PO_{70}EO_{20}$, MW = 5800, Aldrich) dissolved in a HCl solution (0.3 M).[10] The silica source was TEOS (ACROS 98%). The molar composition of the starting reaction mixture was 0.0012 P123 / 0.069 TEOS / 0.102 HCl / 6.771 H_2O. The reaction temperature with TEOS was fixed at 35 °C and the hydrothermal temperature was 100 °C. A typical preparation of the mesoporous 2-D silica is as follows: 6.71 g of P123 is dissolved in 121.87 g of distilled water and 3.72 g of 37 % wt HCl solution with stirring at 35 °C. After complete dissolution, 14.45 g of TEOS is added at once to the homogeneous clear solution. This mixture is left under vigorous stirring at 35 °C for 24 h. Subsequently, the mixture is aged at 100 °C for 24 h under static conditions. The white precipitated product is filtered hot without washing and dried at 100 °C for 24 h in air. Surfactant-free mesoporous material is obtained after a brief ethanol/HCl washing and subsequent calcination at 550 °C in air.

MCM-41 silica support. Mesostructured MCM-41 silica material was prepared under aqueous basic conditions using Cetyltrimethylammonium bromide CTAB ($CH_3(CH_2)_{15}N(Br)(CH_3)_3$, MW = 365, Aldrich) dissolved in an aqueous solution.[11] The silica source was TEOS (ACROS 98%). The reaction temperature with TEOS was fixed at 25 °C and the hydrothermal temperature was 90 °C. A typical preparation of the mesoporous silica is as follows: 9.65 g of CTAB is dissolved in 480 g of distilled

water with stirring at 35 °C. After complete dissolution, 36.5 mL of NH_4OH solution (29 % weight) is added to the solution. The temperature is reduced at 25 °C. After 15 minutes at 25 °C, 40 g of TEOS is added and the mixture is left under stirring for 2 h. Subsequently, the mixture is aged at 90 °C for 3 days under static conditions. The white precipitated product is filtered hot without washing and dried at 100 °C for 24 h in air. Surfactant-free mesoporous material is obtained after a brief ethanol washing and subsequent calcination at 550 °C in air.

Incorporation of the phosphines. To a suspension of a given silica (0.5 g) in dry dichloromethane (30 mL), chlorodiphenylphosphine (0.5 mL, 2.70 mmol) was added and the resulting mixture was further stirred for 4h at 40 °C. After filtration, the resulting powder was washed 2 times in CH_2Cl_2 for materials **SBA/MCM-Ph** and using Soxhlet extraction for materials **SBA/MCM-Ph-sox**. A white powder was obtained.

*Passivation with hexamethyldisilazane (***SBA*-Ph and MCM*-Ph***).* Hexamethyldisilazane (Sigma-Aldrich 97%) (0.8 mL, 3.9 mmol) was added to a suspension of silica (**SBA-Ph or MCM-Ph**) (0.5 g) in dry toluene (30 mL). The reaction proceeded for 24 h at 110 °C. After cooling, the powder was filtered, washed twice with dry toluene and drying under vacuum.

Characterization. Solid state NMR spectra were recorded with a Bruker Avance 300 MHz spectrometer (^{13}C: 75.4 MHz; ^{31}P: 121.4 MHz; ^{29}Si: 59.6 MHz) equipped with a MAS probe head using 4mm ZrO_2 rotors and a sample spinning rate of 8000 Hz. The NMR spectra were recorded using cross-polarization/magic angle spinning (^{13}C) or magic angle spinning (^{29}Si and ^{31}P). Infrared spectra were recorded using a Thermo-Nicolet Magna 850 FTIR spectrometer with a narrow band MCT detector and a diamond ATR Golden-Gate accessory (Specac Ltd., London). The spectra were obtained from 128 scans with a $4cm^{-1}$ resolution.

The elemental analysis was performed at Midwest Microlab, LLC. Carbon, Hydrogen was performed on the Exeter Analytical CE-440 Analyzer. This method involves combustion of the sample at 1000 °C, in the presence of Sn under ultra-pure oxygen. The resulting gases are passed through a copper tube at 670 °C to scrub the excess oxygen from the reaction. The final gasses CO_2 and H_2O are read by a thermal conductivity detector. Certified NIST standards of Acetanalide, Cyclohexanone and 2,4-Dinitrophenyl hydrazone were used for calibration of the instrument prior to any determinations. The method error is +/- 0.30% absolute on both carbon and hydrogen. The method used for chlorine determination is by Schoeninger flask combustion and subsequent titration with $AgClO_4$. The method error for chlorine is +/- 0.40% absolute. *Para*-chloro-benzoic Acid was used for calibration. Nitrogen adsorption-desorption isotherms were measured at liquid nitrogen temperature (-196 °C) using a Quantachrome Autosorb-1MP volumetric adsorption analyser. Before the measurements, the samples were outgassed under vacuum for 24h at 200 °C. The Brunauer-Emmett-Teller (BET) equation was used to calculate the apparent surface area from adsorption data obtained at P/P_0 between 0.05 and 0.2. Total pore volume of micro-mesopores was calculated from the amount of nitrogen adsorbed at $P/P_0 = 0.95$, assuming that adsorption on the external surface was negligible compared to adsorption in pores. The pore size distributions were determined by using *non-local density functional* (NLDFT) methods considering sorption of nitrogen at -196 °C in cylindrical silica pores. Both the kernel of equilibrium NLDFT isotherms (desorption branch) and the kernel of (metastable) NLDFT adsorption isotherms (adsorption branch) were applied for pore width determination.[12]

DFT Methodological details

All DFT calculations were performed with Gaussian 03[18]. Calculations were carried out at the DFT level of theory using the hybrid functional B3PW91[19]. Geometry optimizations were achieved without any

symmetry restriction. Calculations of vibrational frequencies were systematically done in order to characterize the nature of stationary points. Stuttgart effective core potentials and their associated basis set were used for silicon atoms[20]. The basis sets were augmented by a set of polarization functions (ζd=0.284). Hydrogen, Carbon, Oxygen and Phosphorous atoms were treated with 6-31G(d,p) double-ζ basis sets[21].

The optimized structures were used for $^{\{31\}}$P NMR calculations. In all cases, among the various theories available to compute chemical shielding tensors, the Gauge Including Atomic Orbital (GIAO) method has been adopted for the numerous advantages it presents[22]. Typically, in order to compare our calculations with experimental values, $^{\{31\}}$P chemical shielding has been converted to chemical shift using the usual equation: $\delta_{iso} = \sigma_{iso}(ref) - \sigma_{iso}(sample)$ where $\sigma_{iso}(ref)$ is the isotropic $^{\{31\}}$P chemical shielding of phosphoric acid calculated at the same level that the studied systems : $\sigma_{iso}(ref) = 380.5993$ ppm.

AUTHOR INFORMATION

Corresponding Authors

frederic.fontaine@chm.ulaval.ca; freddy.kleitz@chm.ulaval.ca; laurent.maron@irsamc.ups-tlse.fr

Acknowledgements

The authors acknowledge financial support from the National Science and Engineering Research council (Canada), the Canadian Foundation for Innovation and the *Fonds québécois de la recherche sur la nature et les technologies* (Province of Quebec). L.M. is member of the *Institut Universitaire*

de France. CINES and CALMIP are acknowledged for generous grant of computing time. The authors wish to thank Prof. Michel Pézolet and Jean-François Rioux (Department of Chemistry, Université Laval) for the access to ATR-IR measurements and Rémy Guillet-Nicolas (Department of Chemistry, Université Laval) for providing the nitrogen adsorption-desorption data of the silica supports.

Supporting Information Available: Nitrogen adsorption-desorption isotherms (measured at -196°C) of SBA-15 and MCM-41, ^{13}C and ^{29}Si MAS NMR of synthesized compounds, and full details on the DFT models used in this study. This information is available free of charge via the Internet at **http://pubs.acs.org**.

References

(1) (a) Mendonca, A. in *Power of Functional Resins in Organic Synthesis*; Tulila-Puche, J. and Albericio, F. Eds.; VCH-Wiley, Weinheim, Germany, 2008, pp 227-243. (b) Anwander, R. in *Handbook of Heterogeneous Catalysis, 2nd edition*, Ertl, G.; Knötzinger, H.; Schüth, F.; Weitkamp, J. Eds., VCH-Wiley, Weinheim, 2008, Vol. 1, pp 583-614. (c) McNamara, C. A.; Dixon, M. J.; Bradley, M. *Chem. Rev.* **2002**, *102*, 3275-3300. (d) Buchmeister, M. R. *Chem. Rev.* **2009**, *109*, 303-321. (e) McEleney, K.; Allen, D. P.; Holliday, A. E.; Crudden, C. M. *Org. Lett.* **2006**, *8*, 2663-2666. (f) Crudden, C. M.; McEleney, K.; MacQuarrie, S. L.; Blanc, A.; Sateesh, M.; Webb, J. D. *Pure Appl. Chem.* **2007**, *79*, 247-

260. (g) Feng, X.; Fryxell, G. E.; Wang, L. Q.; Kim, A. Y.; Liu, J.; Kemner; K. M. *Science* **1997**, *276*, 923-926.

(2) (a) Anderson, E. B.; Buchmeiser, M. R. *ChemCatChem* **2012**, *4*, 30-44. (b) Das, M. C.; Xiang, S.; Zhang, Z.; Chen, B. *Angew. Chem., Int. Ed.* **2011**, *50*, 10510-10520. (c) Van Doorslaer, C.; Wahlen, J.; Mertens, P.; Binnemans, K.; De Vos, D. *Dalton Trans.* **2011**, *39*, 8377-8390. (d) Martin-Aranda, R. M.; Čejka, J. *Top. Catal.* **2010**, *53*, 141-153. (e) De Vos, D. E.; Dams, M.; Sels B. F.; Jacobs, P. A. *Chem. Rev.* **2002**, *102*, 3615-3640. (f) Lu, Z. L.; Lindner E.; Mayer, H. A. *Chem. Rev.* **2002**, *102*, 3543-3578. (g) Copéret, C.; Chabanas, M.; SaintArroman; R. P.; Basset, J.-M. *Angew. Chem., Int. Ed.* **2003**, *42*, 156-181.

(3) (a) Ying, J. Y.; Mehnert, C. P.; Wong, M. S. *Angew. Chem. Int. Ed.* **1999**, *38*, 56-77. (b) Song, C. E.; Lee, S. *Chem. Rev.* **2002**, *102*, 3495-3524. (c) Wight, A. P.; Davis, M. E. *Chem. Rev.* **2002**, *102*, 3589-3614. (d) Taguchi, A.; Schuth, F. *Microporous Mesoporous Mater.* **2005**, *77*, 1-45. (e) Corma, A.; Garcia, H. *Adv. Synth. Catal.* **2006**, *348*, 1391-1412. (f) S. Minakata, M. Komatsu, *Chem. Rev.* **2009**, *109*, 711-724.

(4) a) Soler-Illia, G. J. A. A.; Patarin, J.; Lebeau, B. ; Sanchez, C. *Chem. Rev.* **2002**, 102, 4093. b) Antonietti, M.; Ozin, G.A. *Chem. Eur. J.* **2004**, *10*, 28-41. c) Tagushi, A.; Schüth, F. *Microporous Mesoporous Mater.* **2004**, *77*, 1. d) Schüth, F. *Annu. Rev. Mater. Res.* **2005**, *35*, 209-238. e) Wan, Y.; Zhao, D. *Chem. Rev.* **2007**, *107*, 2821-2860.

(5) Few leading references: (a) Wang, L.; Dehe, D.; Philippi, A.; Ernst, S.; Zhou, Z.; Hartmann, M.; Taylor, R. N. K.; Singh, A. P.; Jia, M.; Thiel, W. R. *Catal. Sci. Technol.* **2012**, *2*, 1188-1195. (b) Hamasaka, G.; Ochida, A.; Hara, K.; Sawamura, M. *Angew. Chem. Int. Ed.* **2007**, *46*, 5381-5383. (c)

Carniato, F.; Gatti, G.; Gervasio, G.; Marabello, D.; Sappa, E.; Secco, A. *Inorg. Chim. Acta* **2010**, *363*, 1773-1778. (d) Kwon, B. J.; Ku, J. Y.; Yu, K. H.; Ko, J. E.; Jung, H. *J. Phys. Chem. Solids* **2010**, *71*, 663-668. (e) Genelot, M.; Dufaud, V.; Djakovitch, L. *Tetrahedron* **2011**, *67*, 976-981. (f) Sayah, R.; Le Floch, M.; framer, E.; Dufaud, V. *J. Mol. Catal. A* **2010**, *315*, 51-59.

(6) Bluemel, J. *Coord. Chem. Rev.* **2008**, *252*, 2410-2423.

(7) Blanc, F.; Thivolle-Cazat, J.; Basset, J.-M.; Copéret, C.; Hock, A. S.; Tonzetich, Z. J.; Schrock, R. R. *J. Am. Chem. Soc.* **2007**, *129*, 1044-1045.

(8) Smet, P.; Verpoort, F.; De Doncker, G.; Bossuyt, A. R.; Fiermans, L.; Verdonck, L. *Appl. Spectro.* **1997**, *50*, 1807-1813.

(9) Morrow, B. A. ; Lang, S. J. *J. Phys. Chem.* **1994**, *98*, 13319-13322.

(10) Choi, M.; Heo, W.; Kleitz, F.; Ryoo, R. *Chem. Commun.* **2003**, 1340–1341.

(11) (a) Grün, M.; Unger, K.K.; Matsumoto, A.; Tsutsumi, K. *Microporous Mesoporous Mater.* **1999**, *27*, 207-216. (b) Kleitz, F; Schmidt, W.; Schuth, F. *Microporous Mesoporous Mater*. **2003**, *65*,1-29.

(12) (a) Neimark, A.V. Ravikovitch, P. I. *Microporous Mesoporous Mater.* **2001**, *44*, 697-707. (b) Ravikovitch, P. I.; Neimark, A. V. *Colloids Surf. A: Phys. Eng. Aspects* **2001**, *187*, 11-21. (c) Ravikovitch, P. I.; Neimark, A. V. *J. Phys. Chem. B* **2001**, *105*, 6817-6823. (d) Thommes, M. in Nanoporous Materials; Science and Engineering; Lu, G. Q.; Zhao, X.S., Eds.; Imperial College Press: London, U.K., 2004, pp 317-364. (e) Neimark, A. V.; Ravikovitch, P. I.; Vishnyakov, A. *J. Phys. Condensed Matter.* **2003**, *15*, 347-365. (f) Kleitz, F.; Bérubé, F.; Guillet-Nicolas, R.; Yang C.-M.; Thommes, M. *J. Phys. Chem. C* **2010**, *114*, 9344-9355.

(13) (a) Del Rosal, I.; Gerber, I. C.; Poteau, R.; Maron, L. *J. Phys. Chem. A* **2010**, *114*, 6322–6330.

(14) (a) Staub, H.; Guillet-Nicolas, R.; Even, N.; Kayser, L; Kleitz, F.; Fontaine, F.-G. *Chem. Eur. J.* **2011**, *17*, 4254-4265. (b) Yang, Y.; Beele, B.; Bluemel, J. *J. Am. Chem. Soc.* **2008**, *130*, 3771-3773.

(15) While MCM-41 has a higher content of $(RO)_3Si(OH)$ than SBA-15, the later material possess more structural defects and $(RO)_2Si(OH)_2$ than MCM-41, which gives larger silanol content. See reference: Shenderovich, I. G.; Mauder, D.; Akcakayiran, D.; Buntkowsky, G.; Limbach, H.-H.; Findenegg, G. H. *J. Phys. Chem. B.* **2007**, *111*, 12088-12096.

(16) On these materials, no reliable phosphorous content could be monitored since silica was found to interfere with the reliability of the measurements.

(17) Alonso, E.; Sherman, A. M.; Wallington, T. J.; Everson, M. P.; Field, F. R.; Roth, R.; Kirchain, R. E. *Environ. Sci. Technol*. **2012**, *46*, 3406−3414.

(18) Frisch, M. J. *et al.* Gaussian 03 (Revision B.05), **2003**.

(19) (a) Perdew, J. P. in *Electronic structure of solids* ; Ziesche, P. ; Eschrig, H. Eds.; Akademie: Berlin, 1991. (b) Perdew, J. P.; Burke, K.; Wang, Y. *Phys. Rev. B* **1996**, *54*, 16533-16539. (c) Burke, K.; Perdew, J. P.; Wang, Y. in *Electronic density functional theory: recent progress and new directions*; J. F. Dobson, G. Vignale, M. P. Mas, Eds.; Plenum: New-York, 1998. (d) Perdew, J. P.; Chevary, J. A.; Vosko, S. H.; Jackson, K. A.; Pederson, M. R.; Singh, D. J.; Fiolhais, C. *Phys. Rev. B* **1992**, *46*, 6671-6687. (e) Perdew, J. P.; Burke, K.; Wang, Y. *Phys. Rev. B* **1998**, *57*, 14999. (f) Perdew, J. P.; Chevary, J. A.; Vosko, S. H.; Jackson, K. A.; Pederson, M. R.; Singh, D. J.; Fiolhais, C. *Phys. Rev. B*, **1993**, *48*, 4978.

(20) Küechle, W.; Dolg, M. ; Stoll, H.; Preuss, H. *Mol. Phys.*, **1991**, *74*, 1245-1263.

(21) (a) Harihara, P. C.; Pople, J. A. *Theo. Chim. Acta*, **1973**, *28*, 213-222. (b) Hehre, W. J.; Ditchfield, R.; Pople, J. A. *J. Chem. Phys.*, **1972**, *56*, 2257-2261.

(22) (a) Wolinski, K. ; Hilton, J. F.; Pulay, P. *J. Am. Chem. Soc.* **1990**, *112*, 8251-8260. (b) McWeeny, R. *Phys Rev.* **1962**, *126*, 1028-1034. (c) London, F. J. *Phys. Radium* **1937**, *8*, 397-409. (d) Dodds, J. L.; McWeeny, R.; Sadlej, A. J. *Mol. Phys.* **1980**, *41*, 1419-1430. (e) Ditchfield, R. *Mol. Phys.* **1974**, *27*, 789-807. (f) Junk, P. C.; Steed, J. W. *J. Organomet. Chem.* **1999**, *587*, 191.

FIGURES

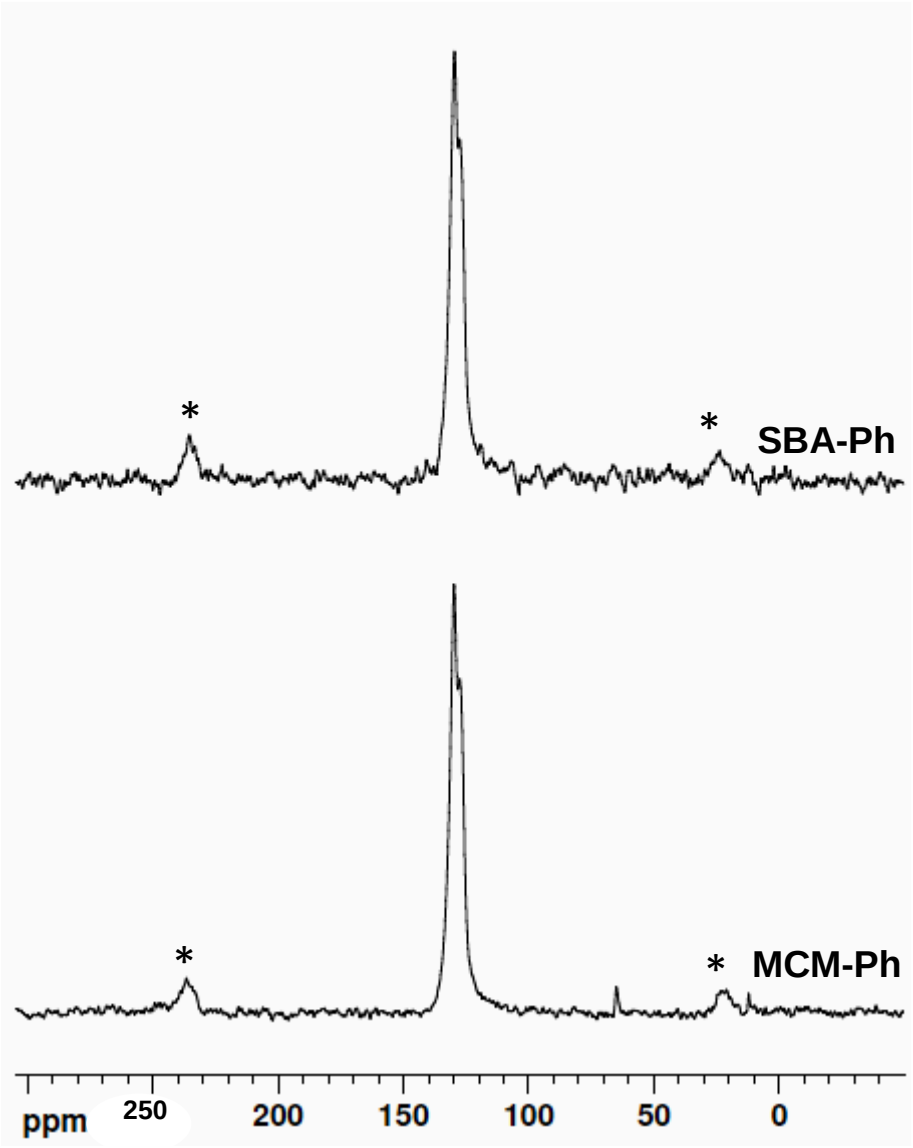

Figure 1. $^{13}C\{^{1}H\}$ CP/MAS NMR spectra of the SBA-Ph and MCM-Ph materials, as indicated.

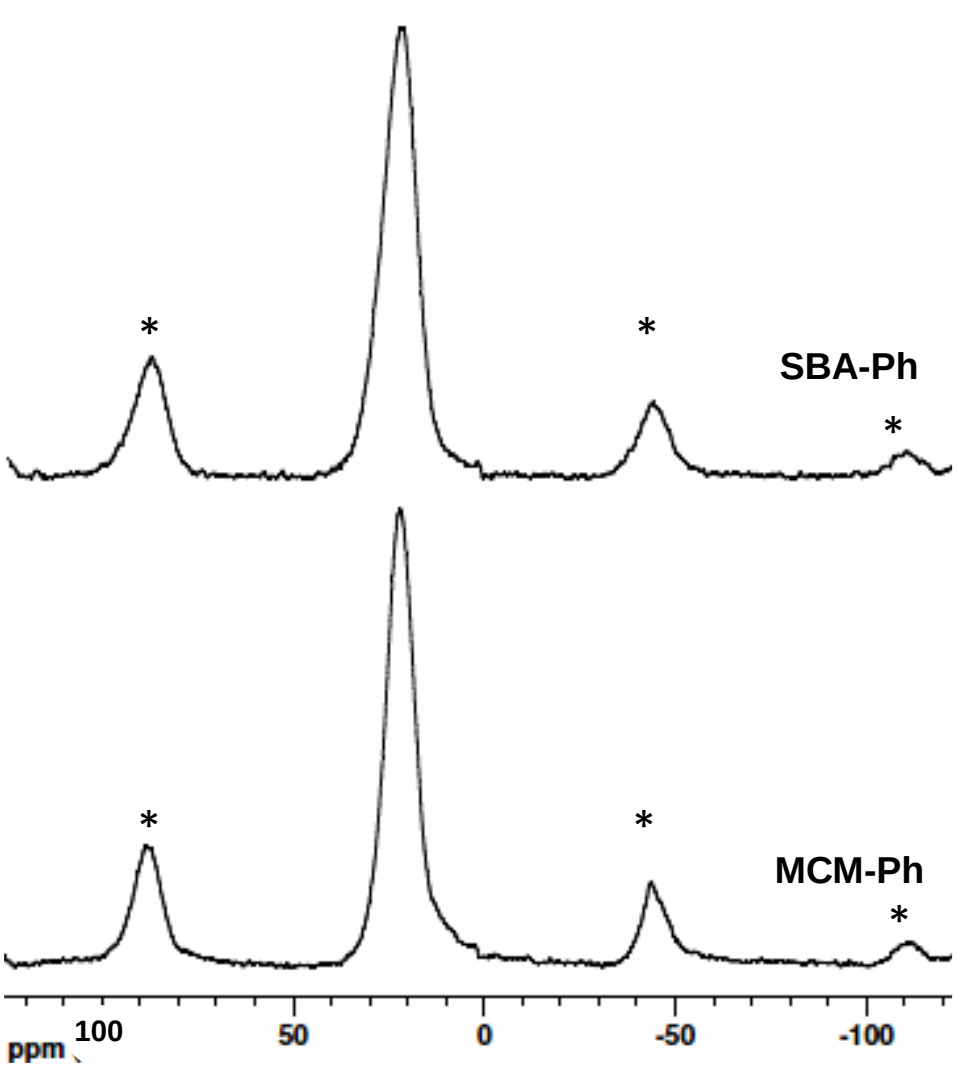

Figure 2. $^{31}P\{^{1}H\}$ MAS NMR spectra of SBA-Ph and MCM-Ph materials, as indicated.

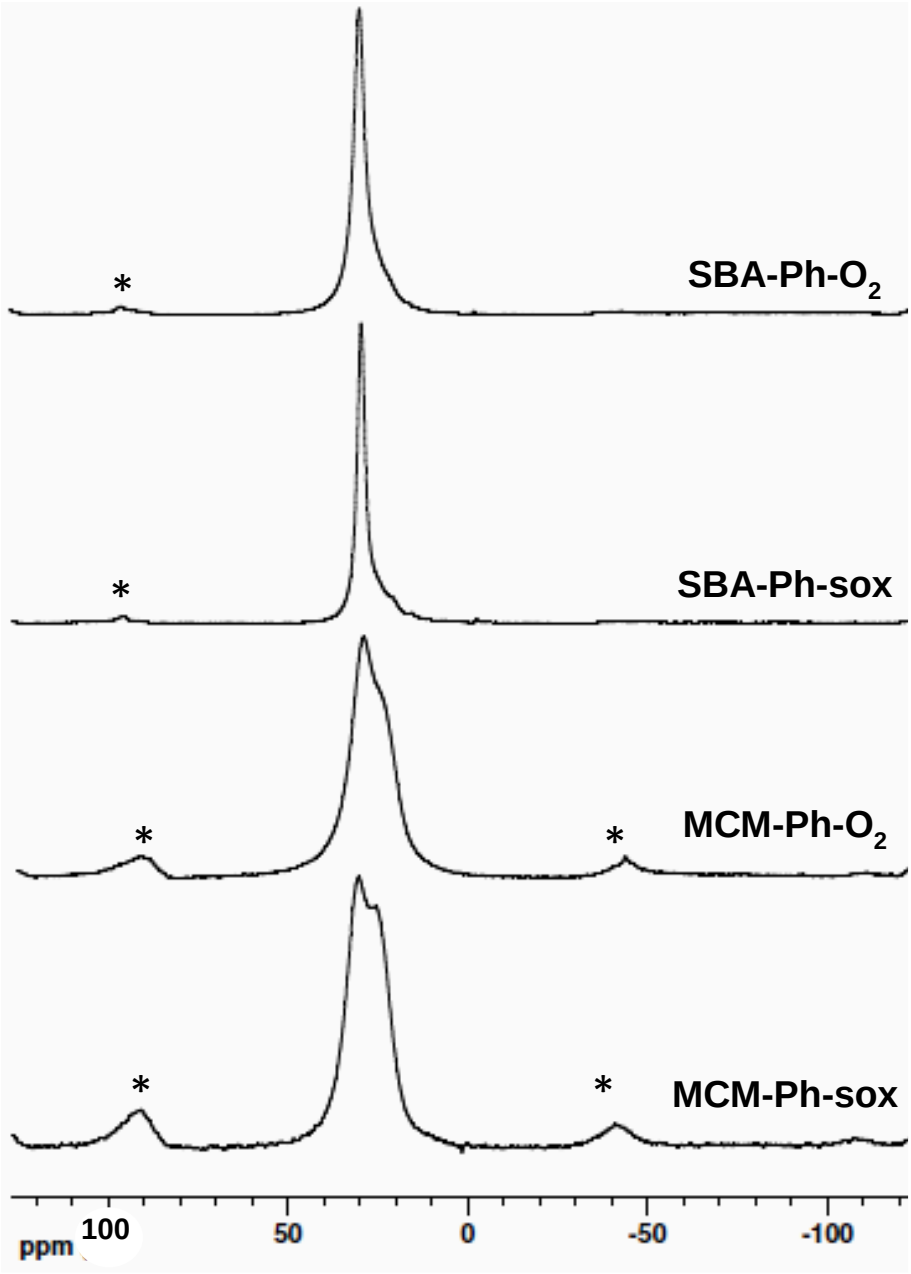

Figure 3 $^{31}P\{^{1}H\}$ MAS NMR spectra of SBA-Ph-O_2, SBA-Ph-sox, MCM-Ph-O_2 and MCM-Ph-sox materials, as indicated.

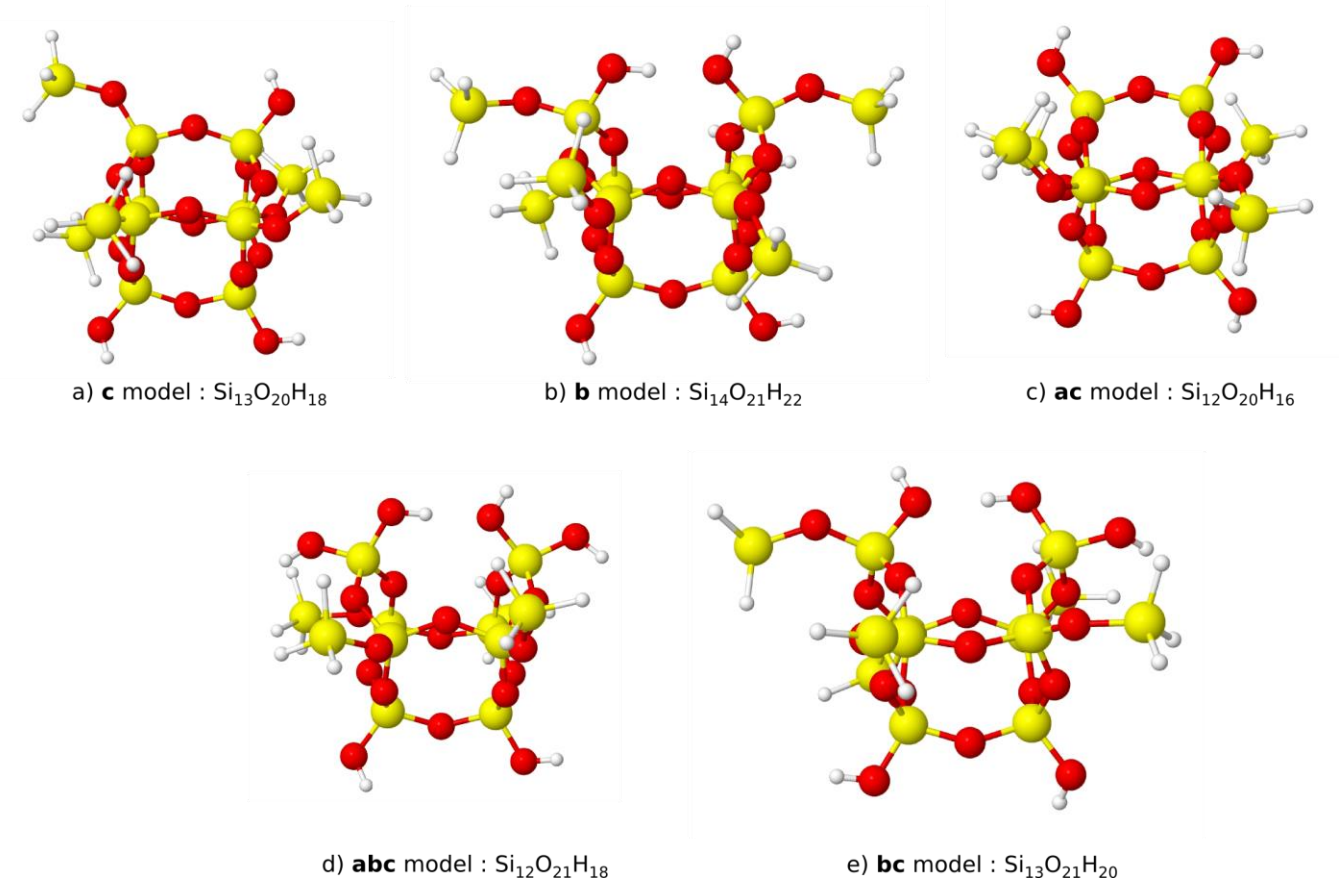

Figure 4. Definition and nomenclature of the models used to represent mesoporous silica.

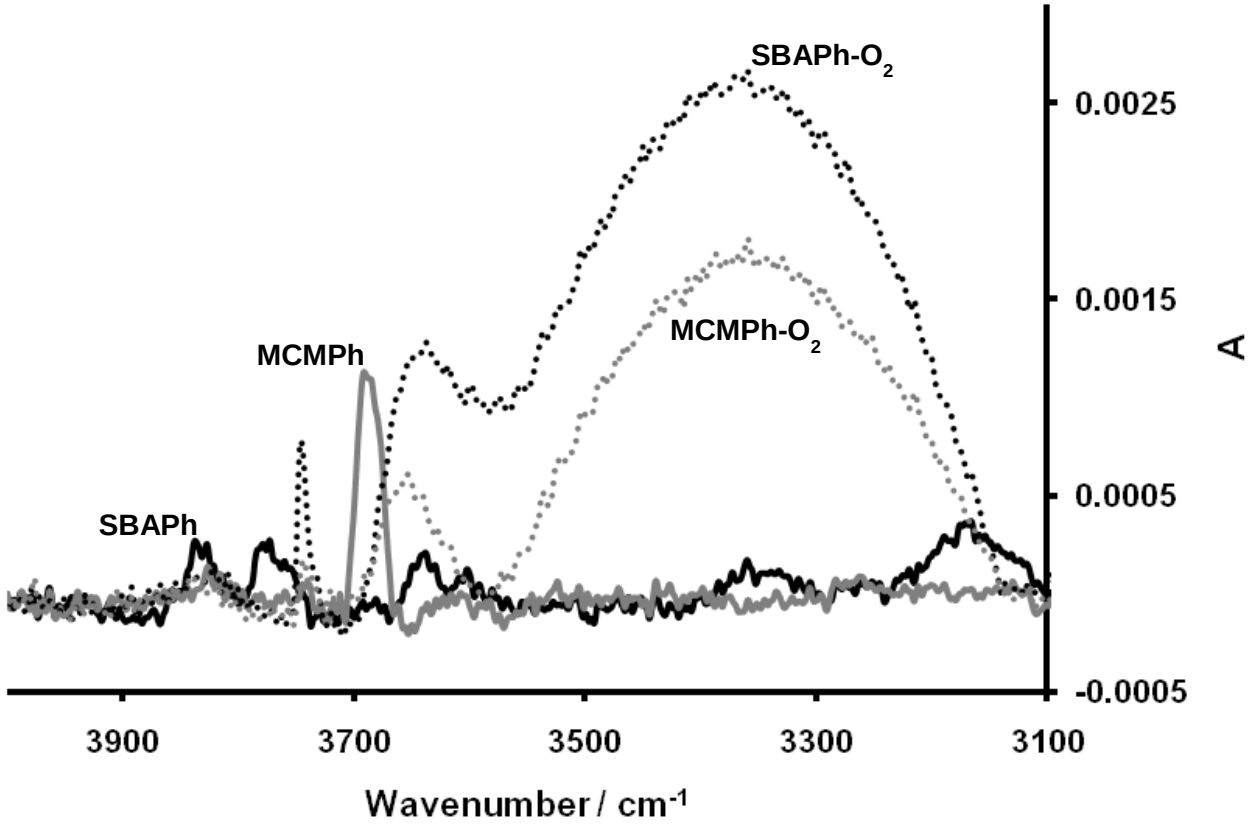

Figure 5. Selected region of the ATR-IR corresponding to the water and silanol vibrational modes of the selected materials prior (solid line) and after exposure to air (dotted line).

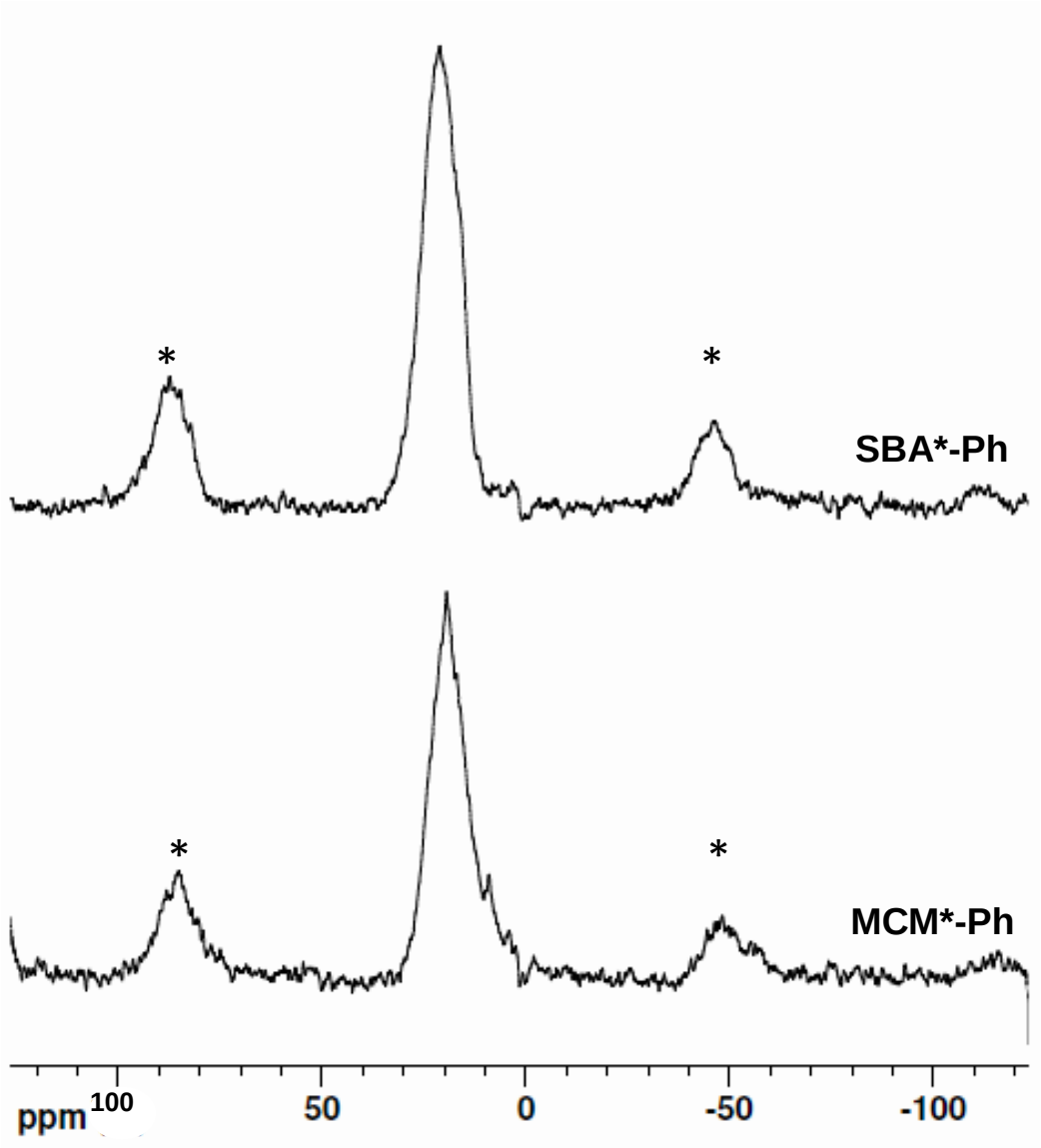

Figure 6. $^{31}P\{^{1}H\}$ MAS NMR spectra of SBA*-Ph and MCM*-Ph materials, as indicated.

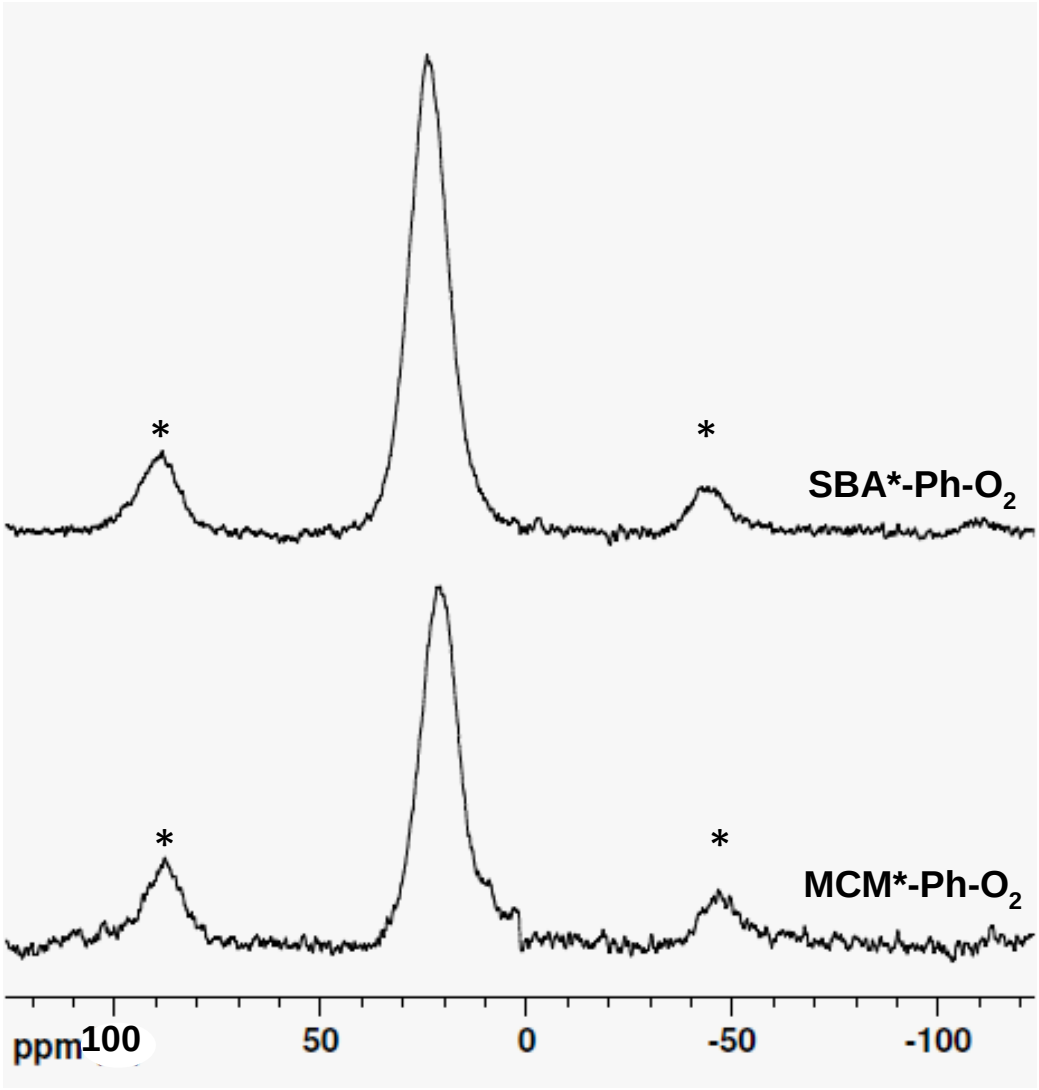

Figure 7. $^{31}P\{^{1}H\}$ MAS NMR spectraof SBA*-Ph-O_2 and MCM*-Ph-O_2 materials, as indicated.

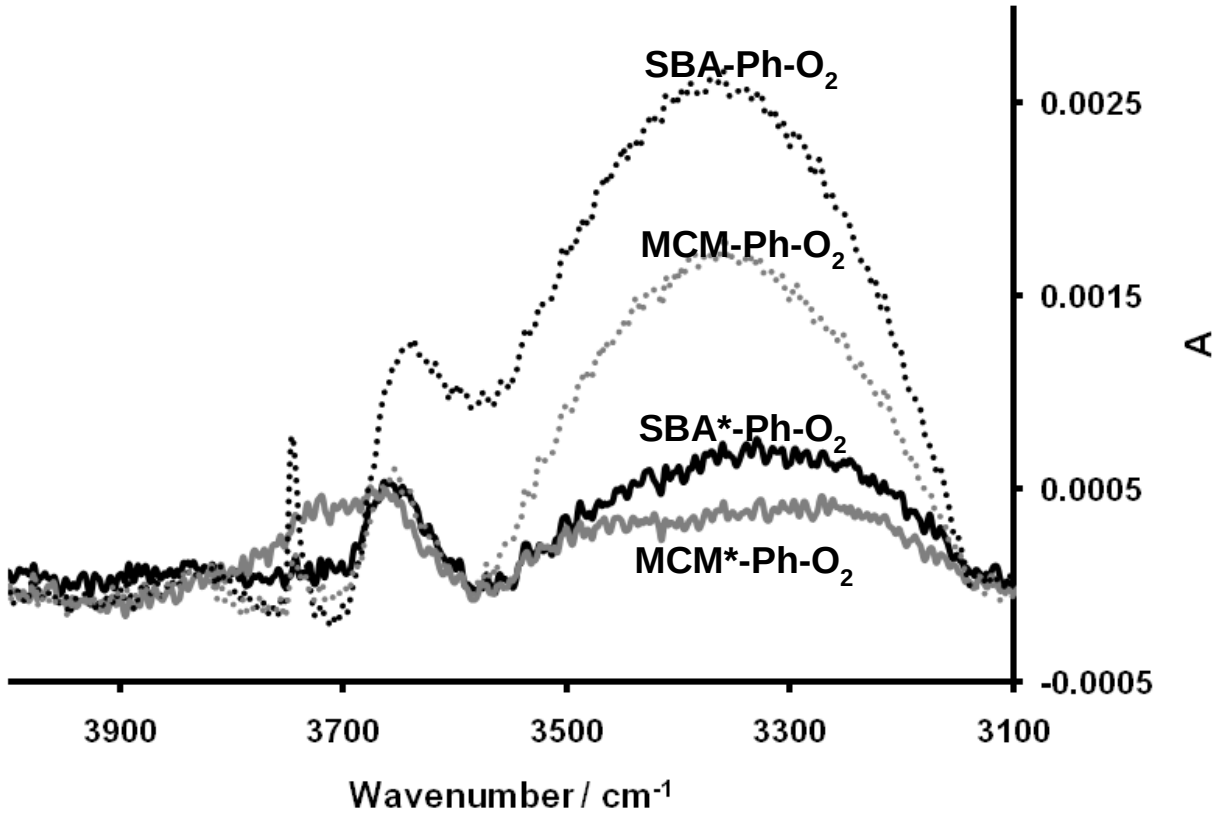

Figure 8. Selected region of the ATR-IR corresponding to the water and silanol vibrational modes of the selected materials after exposure to air, before (solid line) and after passivation (dotted line).

TOC

On the Interaction of Phosphines with High Surface Area Mesoporous Silica

Hélène Staub, Iker Del Rosal, Laurent Maron, Freddy Kleitz* and Frédéric-Georges Fontaine**